Journal of Materials Chemistry A

Accepted Manuscript

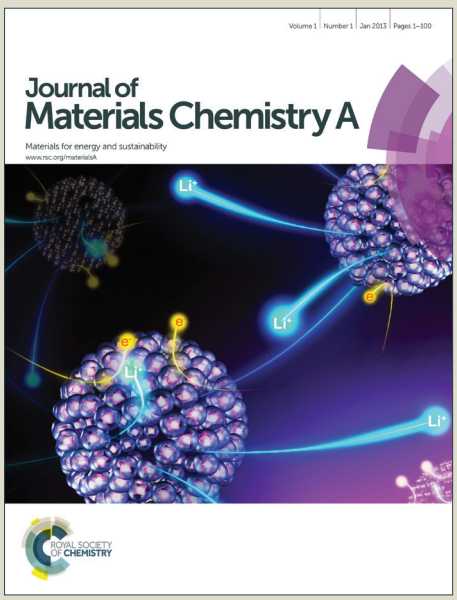

ROYAL SOCIETY OF CHEMISTRY

www.rsc.org/materialsA

J. Mat.Chem. A

ARTICLE

Highly stable ruthenium nanoparticles on 3D mesoporous carbon: An excellent opportunity for the reduction reactions†

Received 00th January 20xx,
Accepted 00th January 20xx

DOI: 10.1039/x0xx00000x

www.rsc.org/

Pitchaimani Veerakumar,[a,*] Namasivayam Dhenadhayalan,[b] King-Chuen Lin[b] and Shang-Bin Liu [*a,c]

Abstract: Carbon mesoporous materials (CPMs) have great potential in the field of heterogeneous catalysis. Highly dispersed ruthenium nanoparticles (RuNPs) embedded on three dimensional (3D) CPMs as catalysts with high surface area (1474 m^2 g^{-1}) were prepared by microwave-thermal reduction processes. Characterization technologies including X-ray diffraction (XRD), N_2 adsorption/desorption isotherm measurements, field emission transmission electron microscopy (FE-TEM), thermogravimetric analysis (TGA), hydrogen temperature-programmed reduction (H_2-TPR), Raman spectroscopy and solid state magic angle spinning NMR spectra nuclear magnetic resonance (^{13}C MAS NMR) were utilized to scrutinize the catalysts. It was revealed that the Ru/CPMs catalysts exhibited highly ordered 3D mesoporous structure and large surface area and widely uses as catalyst for the reduction reactions. Reduction of *p*-nitroaniline (*p*-NA) and crystal violet (CV) by $NaBH_4$ with the use of this catalyst was studied by means of UV–Vis spectroscopy. Here, $NaBH_4$ acting as hydrogen donor. This catalyst shows an excellent catalytic activity towards reduction of *p*-NA and CV dye at room temperature. Due to their promising properties of CPM, it can be utilized to fabricate 3D carbon-based materials for a variety of novel applications.

1. Introduction

Metal-incorporated carbon porous materials (CPMs) have been vastly studied, they are very attractive in the field of adsorption, separation, sensors, catalysis, energy storage and hydrogen storage applications during the last several years.[1–3] It exhibits several unique properties such as large specific surface area (SSA), large pore volume, well-ordered mesoporous structure and high stablity.[4] Recently, Dai group reported a versatile synthesis of high surface area CPMs, based on the evaporation induced self-assembly (EISA) method followed by soft-templating principle using phenolic resins as carbon precursors (phenol-, resorcinol-/phloroglucinol) and triblock copolymer (F127) as the structural directing agent.[5] Ordered porous carbon materials can be successfully synthesized through different pathways.[2a] The main constituents of block copolymer and resols (phenol, resorcinol, or phloroglucinol/formaldehyde/glyoxal/glyoxalicacid/terephthalaldehyde) has been demonstrated as one of the efficient path way for the synthesis of mesoporous carbons with well-organized mesostructures.[6] It is due to enhanced hydrogen-bonding interaction between three hydroxyl groups of phloroglucinol and triblock copolymers. In recent years, ruthenium nanoparticles (RuNPs) often has a significant influence on its catalytic property due to its size, shape, and structure.[7] It is a well-known catalysts used for a wide range of organic reactions, such as Fischer–Tropsch (FT) synthesis,[8] ammonia synthesis,[9] oxidation,[10,11] reduction,[12] C–C coupling reactions[13] and so on.

One of the most important advantages and very attractive applications offered by microwave-assisted synthesis of mesoporous carbon over the conventional methods such as (i) facile control of porosity and surface area, (ii) increased product yield and purity, (iii) reduced reaction time and operation cost, and (iv) feasibility for mass production.[14–15] Therefore, microwave radiation technique was used synthesis of mesoporous multidimensional wormhole-like carbons,[3c,d] carbon-gels,[14a–c] carbon-xerogel spheres,[14d,e] ordered mesoporous carbon[15a,b] mesoporous carbon-cubes[15c] etc.

In recently, the catalytic reduction of aromatic nitro compounds by sodium borohydride ($NaBH_4$) in the presence of

[a] Institute of Atomic and Molecular Sciences, Academia Sinica, Taipei, 10617 Taiwan) Fax: (+886) 2-23620200) Emails: spveerakumar@gmail.com (P.Veerakumar); sbliu@sinica.edu.tw
[b] Department of Chemistry, National Taiwan University and Institute of Atomic and Molecular Sciences, Academia Sinica, Taipei 106, Taiwan.
[c] c Department of Chemistry, National Taiwan Normal University Taipei 106, Taiwan.

† Electronic supplementary information (ESI) available: UV-Vis studies. See DOI: 10.1039/x0xx00000x

metal nanoparticles has made great progress.[16] In particular, the reduction of *p*-nitroaniline (*p*-NA) to *para*-phenylenediamine (*p*-PDA), which is mainly used as an ingredient in dyes, rubber antioxidants, curing agents for epoxy resin and is also a precursor to aramid textile fibers, thermoplastics and cast elastomers.[17] Therefore, developing a general, economic and simple route to preparation of *p*-PDA is still of great interest and importance in many industrial chemicals.

Generally, water soluble dyes (acidic, basic, neutral, azo, directive, reactive and so on) are possess a major threat to the surrounding ecosystem, that are extensively used in textile dyeing, paper colouring, and paint industries.[18] Among them, a typical cationic triphenylmethane dyes are most widely used for biological stain, a dermatological agent, a veterinary medicine, an additive to poultry feed to inhibit propagation of mold, intestinal parasites and fungus.[19] Especially, crystal violet (CV), which has been used to identify the bloody fingerprints in human and domestic animals and also used as an adhesive taps for latent printing. They are extremely toxic to mammalian cells, antimicrobial, mitotic poison and mutagenic. It may cause cancer, severe eye irritation, harmful by inhalation, ingestion and through skin contact.[20] Therefore, CV was chosen as the model pollutant dye in this research. Thus, we focus on the removal of dye from the water bodies, becomes essential and still are scarce.[21,22] Compared to CV, the LCV (*i.e* completely reduced form of CV) is less toxic, colorless stable under normal conditions. Therefore, such type of colorless compounds can be used forensic agencies in worldwide, particularly large crime scene areas in most scenarios.[23]

Herein, we report the synthesis of high-quality 3D ordered mesoporous carbons incorporated with highly dispersed uniform RuNPs as detailed in Scheme 1. These catalysts have high surface area and were used as catalyst for the reduction reactions. Reduction reaction of *p*-NA and CV using $NaBH_4$ as reductant was investigated and monitored by UV–visible spectroscopy.

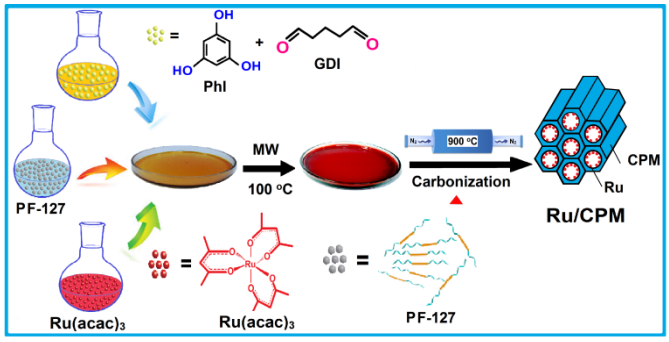

Scheme 1 Schematic illustrations for the synthesis of Ru/CPMs catalysts.

2. Experimental section

2.1 Materials and reagents

A triblock copolymer surfactant (PF-127), pluronic F-127 (PF-127, PEO_{106}-PPO_{70}-PEO_{106}, Mw = 12600, Sigma-Aldrich), phloroglucinol (Phl, 99%, Acros), glutaric dialdehyde (GDI, 25 wt% in H_2O, Sigma-Aldrich) and ruthenium(III) acetylacetonate ($Ru(C_5H_7O_2)_3$, 97%, Strem Chemicals, Inc.) were purchased. Research grade *p*-nitroaniline and sodium borohydride were obtained from Fisher Scientific. The crystal violet dye was obtained from Sigma-Aldrich with analytical grade. Millipore water with resistivity 18 MΩ/cm was used for all reactions and purifications.

2.2 Sample preparation

Resol precursor was prepared by the polymerization of phloroglucinol and formaldehyde under an acidic environment as described previously.[3d,20] As illustrated in Scheme 1, the typical synthesis: phloroglucinol (3.75 g) and pluronic F127 (4.0 g) were dissolved in an equal volume of ethanol and water (C_2H_5OH:H_2O, 9.0 mL) solution under constant stirring at below room temperature. Then, upon complete dissolution of the mixture, ~15 drops of conc. HCl (37%) was slowly added till the appearance of light pink color, followed by dropwise addition of 3.7 mL of glutaric dialdehyde into the above solution. After stirring for about ~10-15 min at RT, the clear mixture turned turbid, indicating the formation of Phl-GDI-PF127 polymeric phase. The light yellow coloured phase was centrifuged at 4500 rpm for *ca.* 10 min, while the ethanol and water discarded. Subsequently, the polymeric product was dissolved in desirable amount of $Ru(acac)_3$ (73.9 mg for 0.5 wt% loading; 147.8 mg for 1.0 wt% loading) in 5 mL tetrahydrofuran (THF) to get the clear red color solution. The polymeric gel was then loaded on a large petri dish, dried at RT overnight, then cured at 80 °C (typically for 2 h) and then subjected to microwave irradiation (MW power: 300W, 2-3 h), followed by curing (at 100 °C). During the microwave irradiation the Ru^{3+} ions are effectively reduced to the Ru^0 state and highly dispersed on the mesoporous 3D carbon support. The template was removed thermally by carbonization under N_2 atmosphere at 400 °C for 3 h using a heating rate of 1 °C/min, then at 900 °C for 3 h with a heating rate of 5 °C/min. After carbonization, a natural cooling process was performed. The obtained material was labelled as Ru/CPM-1 and Ru/CPM-2, corresponding to a Ru loading of 0.5 and 1.0 wt%, respectively.

2.3 Catalysts characterization

All powdered X-ray diffraction (XRD) experiments were recorded on a PANalytical (X'Pert PRO) diffractometer using CuKα radiation (λ = 0.1541 nm). Nitrogen porosimetry measurements were carried out with a Quantachrome Autosorb-1 volumetric adsorption analyzer at –196 °C (77 K). Prior to measurement, the sample was purged with flowing N_2 at 150 lC for at least 12 h. The pore size distributions were derived from the adsorption branches of isotherms using the Barrett–Joyner–Halanda (BJH) method. The morphology of the sample was studied by field emission transmission electron microscopy (FE-TEM) at room temperature (25 °C) using an electron microscope (JEOL JEM-2100F) that has a field-emission gun at an acceleration voltage of 200 kV. Elemental compositions of various samples were carried out with an energy-dispersive X-ray (EDX) analyzer (equipped with the FE-TEM). X-ray photoelectron

spectroscopy (XPS) measurements were performed using a ULVAC-PHI PHI 5000 VersaProb apparatus. Thermogravimetric analysis (TGA) was performed on a Netzsch TG-209 instrument under air atmosphere. UV-vis absorption spectral measurements were carried out with a Thermo Scientific evolution 220 UV-visible spectrophotometer. FT-IR spectra were recorded using a Bruker IFS28 spectrometer in the region of 4000–400 cm^{-1} with a spectral resolution of 2 cm^{-1} using dry KBr at room temperature. Hydrogen temperature programmed reduction (H_2-TPR) measurements were performed utilizing a AUTOCHEM-2920 under a flow of 10% H_2/Ar gas mixture and a heating rate of 10 °C/min from room temperature to 900 °C. Prior to the TPR analysis, sample was pre-treated by flowing argon at a flow rate of 30 mL/min at 600 °C for 2 h to remove impurities, then, the system was cooled to room temperature. The amount of H_2 uptake during the reduction was measured continuously with a thermal conductivity detector (TCD). All Raman spectra were recorded on a Jobin Yvon T64000 spectrometer equipped with a charge coupled device (CCD) detector cooled with liquid nitrogen. The backscattering signal was collected with a microscope using an Ar^+ laser centered at 488 nm as the excitation source. ^{13}C magic-angle-spinning (MAS) NMR spectra were recorded by a Bruker Avance 500 NMR spectrometer.

2.4 Catalytic reduction reactions

To study the catalytic properties of the as-synthesized Ru/CPMs, we evaluated the catalytic reduction of dye by $NaBH_4$ in water. In a typical experiment, aqueous solution of 1.7 mL of CV (0.1 mM) was mixed with 0.7 mL of $NaBH_4$ (0.04 M), in a quartz cell (3.0 mL). Then, the catalyst (1 mg) was added into the mixture of CV and $NaBH_4$, and the solution absorbance changes were monitored with a UV-vis spectrophotometer at different time intervals. The original violet colour of the CV was gradually vanished to colourless (LCV). In addition, the reduction of *p*-NA was also carried out under the same conditions.

3. Results and discussion

3.1 Characterization of Ru/CPM catalyst

3.1.1. XRD analysis

The small-angle XRD patterns of pristine CPM and Ru/CPMs catalysts obtained from the PhI-GDI polymeric resin is shown in Fig. 1a. It exhibits an intense peak (100) and two weak peaks (110 and 200) for all samples, which can be attributed to the 3D hexagonal symmetry (*p6mm*) of the ordered mesoporous structures.[6b,22] The high-angle XRD pattern of CPM shows a broad peak at 23.5° and a less intense peak at 43.8° attributed to the (002) and (100) diffraction peaks with limited domain sizes of stacked crystalline graphite structure, respectively (Fig. 1b).[3c] For Ru/CPMs, the peaks observed at 38.3°, 42.2°, 44.0°, 58.3°, 69.4°, and 78.4°are due to the diffractions of the (100), (002), (101), (102), (110), and (103) planes of the hexagonal close-packed (hcp) Ru metal (ICDD-JCPDS card No. 06-0663).[12a] Moreover, a diffraction peak at 44.04° was observed, which could be assigned to the (101) Ru crystallographic planes,[4d] indicating that the RuNPs forms very small particles within the 3D mesoporous carbon matrix.[4e] The average particle size of the RuNPs embedded in 3D carbon matrix was calculated by the Scherrer formula (equ.1),

$$d = 0.9\,\lambda/\beta\cos\theta \qquad (1)$$

where d is the particle size (nm), λ is the wavelength of X-ray used (0.1541 nm), β is the width of the diffraction peak at half height in radians and θ is the diffraction angle at the position of the peak maximum. The calculated average particle size of Ru supported on CPM is *ca.* 3–5 nm, which is consistent with the FE-TEM results (*vide infra*).[12c]

3.1.2 Raman analysis

Fig. 1c represents the Raman spectra of CPM and Ru/CPMs catalyst from 1000–2000 cm^{-1}. The observed two peaks are attributing to the D band (*ca.* 1342 cm^{-1}) and G band (*ca.* 1582 cm^{-1}). The D band is typically representative of disordered carbon (sp^3), corresponding to turbostratic carbon layers or very small graphitic domains; the G band is mainly assigned to in-plane displacement of carbon (sp^2) atoms in hexagonal carbon sheets.[24a] Table 1 shows the lists of the intensity ratio of two bands (I_D/I_G) for the three samples: 0.99 for CPM, 0.96 for Ru/CPM-1, and 0.95 for the Ru/CPM-2 proves the graphitization degree of carbon samples, and a lower value always represents a higher degree of graphitization.[24b]

3.1.3 EDX analysis

The composition of Ru/CPM-2 was determined by energy dispersive X-ray analysis. Analysis through EDX confirms the presence of elemental ruthenium and carbon signals from the Ru/CPM-2 (Fig. 1d). The emission energy measured X-ray signals include the following: C Kα, 0.2 keV; Cu Lα,β, 0.9 keV; Cu Kα, 8.0 keV; Cu Kβ, 8.9 keV; Ru Lα,β, 2.6 keV; Ru Lγ, 3.2 keV; and Ru Kα, 19.2 keV, Cu signals are due to diffuse scattering from the supporting grid.[24c] It suggests that the RuNPs are very evenly distributed in the whole mesoporous 3D carbon matrix.

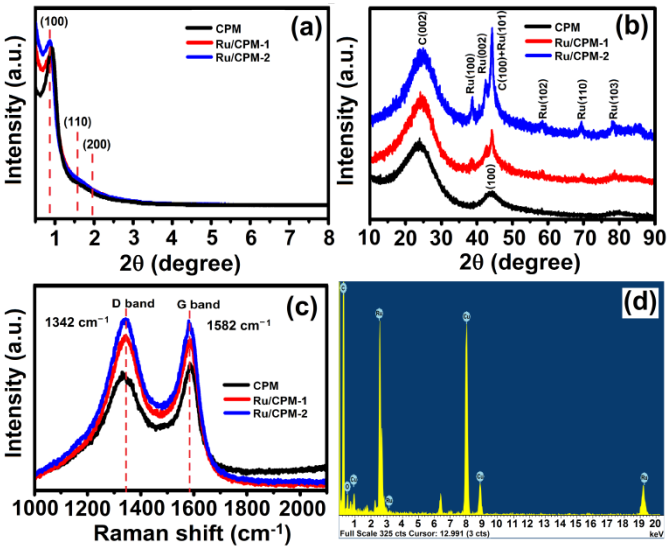

Fig. 1 (a) Small-angle and (b) high-angle XRD patterns, (c) Raman spectra of pristine CPM, Ru/CPM-1, and Ru/CPM-2 catalyst and (d) EDX spectrum of Ru/CPM-2 catalyst.

Table 1 Textural properties of the pristine CPM and Ru/CPM materials

Sample	Ru loading (wt%)	Ru size[a] (nm)	Surface area[b] (m^2 g^{-1})		Pore volume[c] (cm^3 g^{-1})			Pore size[f] (nm)	I_G/I_D
			S_{Total}	S_{Micro}[d]	V_{Total}	V_{Micro}[d]	V_{Meso}[e]		
CPM	–	–	1474	340.4	1.182	0.1506	1.0314	6.22	0.99
Ru/CPM-1	0.1	2.6 ± 0.5	1416	314.5	1.095	0.1440	0.9510	6.17	0.96
Ru/CPM-2	0.5	2.8 ± 0.5	1313	312.0	0.988	0.1401	0.8579	6.12	0.95

[a] Average Ru particle size determined by FE-TEM analysis. [b] Brunauer–Emmet–Teller (BET) surface areas. [c] Total pore volumes calculated as the amount of N_2 adsorbed at P/P_0 = 0.99. [d] Microporous surface areas (S_{Micro}) and pore volumes (V_{Micro}) obtained from *t*-plot analyses. [e] Mesopore volume ($V_{meso} = V_{Total} - V_{micro}$). [f] Pore diameters calculated by the Barrett–Joyner–Halenda (BJH) method using adsorption branches of isotherms.

It suggests that the RuNPs are very evenly distributed in the whole mesoporous 3D carbon matrix.

3.1.4 FE-TEM analysis

The size and morphology of the synthesized CPMs were explored by FE–TEM analysis. As prepared pristine CPMs exhibit highly ordered and well defined mesoporous structures (Fig. 2a & b).[8a] TEM images clearly show that many RuNPs with uniform size of *ca.* 2.6 ± 0.5 nm were highly dispersed and embedded inside the CPMs (Fig. 2c–f). The inset in Fig. 2e shows the electron diffraction pattern of the representative RuNPs. This suggests that RuNPs distributed on CPMs and good agreement with XRD results.[7d]

3.1.5 Surface area analysis

Fig. 3a shows the N_2 adsorption/desorption isotherms of CPM and Ru/CPMs samples, which are carbonized at 900 °C under N_2 atmosphere. These samples exhibit type-IV curves with sharp capillary condensation steps in the relative pressure range (P/P_0) from 0.45–0.65, which is characteristic of a 3D caged a regular mesostructures.[1d,2a] The corresponding surface area, pore volume, pore size, micropore area and micropore volume are summarized in Table 1. All samples exhibited a typical H_1-like hysteresis loop, indicating the mesoporous structure of the materials.[3d,8] The pore size distribution was calculated by the BJH method using adsorption branches of isotherms and calculated around ~5-6 nm as shown in Fig. 3b. The results show that the BET surface areas of Ru/CPM-1 and Ru/CPM-2 were calculated to be 1416 and 1313 m^2 g^{-1}, respectively, which is lower than that of pristine CPM (1474 m^2 g^{-1}), due to the incorporation of RuNPs (Table 1). It suggests that the RuNPs are embedded stably in the inside the mesoporous CPMs.

3.1.6 TGA analysis

Fig. 3c shows thermogravimetric and differential temperature analysis (TG-DTA) curves of CPM and Ru/CPMs catalysts. In TGA curves illustrated a weight loss of 4.6% in the temperature below 100 °C corresponding to removal of water molecules. A very small weight loss (2.75%) between 100–280 °C is attributed to elimination of template (PF-127) surfactant. The third weight loss from 280–800 °C is related to decomposition of CPM framework.[25] From the TGA measurements reveals that the successful incorporation of RuNPs in the mesoporous carbon solid network and confirm high thermal stability of the material.[26]

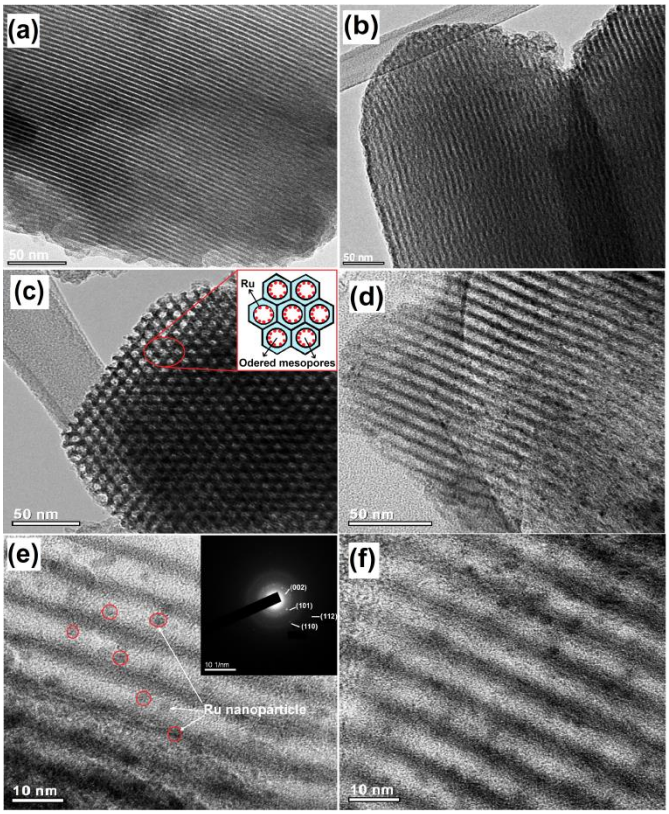

Fig. 2 (a,b) FE-TEM images of pristine CPM, (c,d) Ru/CPM-1 (Inset in (c) show the schematic explanation of a mesoporous 3D Ru/CPM) and (e,f) Ru/CPM-2 catalyst. Inset in (e) show the SAED pattern of the RuNP.

3.1.7 H_2-TPR analysis

To identify the strong interaction between RuNPs and the CPM framework, a series of H_2-TPR treatments of pristine CPM, Ru/CPM-1 and Ru/CPM-2 samples were performed under 5% H_2/Ar. It is an ideal tool for examining the reducibility and interaction between the metal species and support, and also to get information regarding the active state of the solid catalysts.[1c,9b] The H_2-TPR

patterns detected with a thermal conductivity detector are shown in Fig. 3d. Obviously, at lower temperature a small reduction peak *ca.* 210-235 °C was commonly assigned to reduction of trace amount of RuO_2 species (*i.e.*, reduction of RuO_2 to Ru^0).[8a,9a] The second peak at ~525-550 °C was attributed to the methanation of carbon or carbon gasification by H_2 in the presence of the Ru catalyst. Because, ruthenium (Ru) is a good catalyst for the methanation of carbon.[1b]

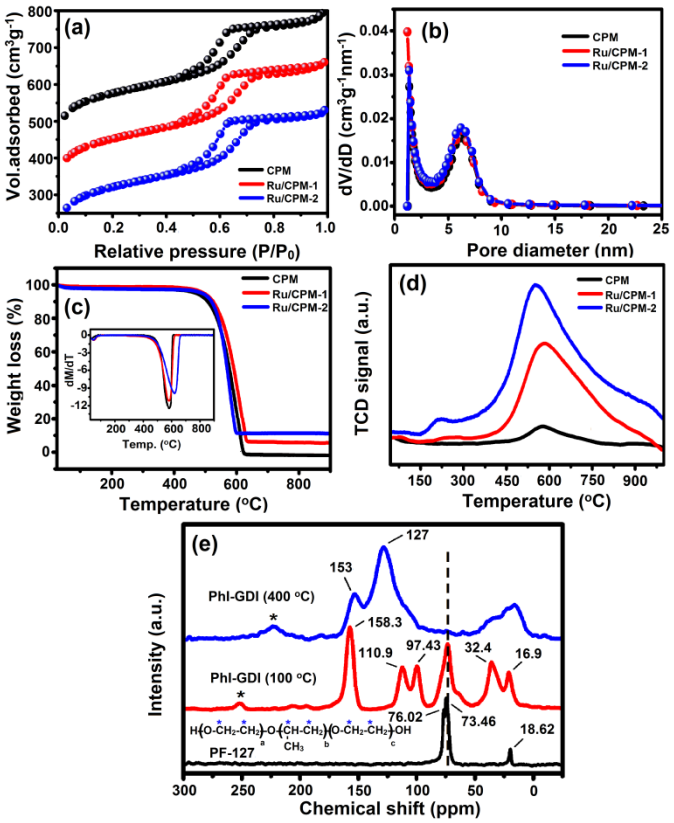

Fig. 3 (a) N_2 sorption isotherms (b) pore size distributions, (c) TG-DTA analysis, (d) H_2–TPR profiles of pristine CPM, Ru/CPM-1, and Ru/CPM-2 catalyst and (e) ^{13}C CP MAS NMR spectra of the pure PF-127, PhI-GDI polymer composite at 100 and 400 °C. The symbol ∗ indicates a spinning sideband.

3.1.8 ^{13}C-NMR analysis

Furthermore, the PhI-GDI frameworks were characterized with solid state magic angle spinning NMR spectroscopy (Fig. 3e). The ^{13}C CP-MAS NMR spectrum of PF-127 shows the strong signals at *ca.*18.62, 73.46, and 76.02 ppm, which are related to the carbon atoms in methyl carbon ($-CH_3$); methylene carbon ($-CH_2$) and methine carbon (-CH), respectively and these carbons are bonded with O atoms in the triblock copolymer.[25,26] After polymerization at 100 °C, the PhI-GDI resin displayed a peak around 153.8 ppm, which is belonged to –OH substituted carbon in PhI, while the chemical shifts at *ca.*110.9 and 97.43 ppm signals can be related to the carbon ($-CH_2-$) atoms in PhI and GDI, respectively. Meanwhile, the signals at *ca.*33.2 and 16.9 ppm could be attributed to methylene linkages between phenolic rings. After pyrolysis at higher temperature (400 °C) the signals of PF-127 disappears, implying that almost all the of triblock copolymer templates are decomposed and removed from the polymeric PhI-GDI carbon matrix. As expected, new signals at *ca.* 153 and 127 ppm are arise from the aromatic carbons directly attached to –OH groups and other aromatic carbons.[27]

3.1.9 XPS analysis

XPS was carried out to further investigate the surface chemical component of the CPM and Ru/CPM-1 with 0.5 wt% Ru (Fig. 4).

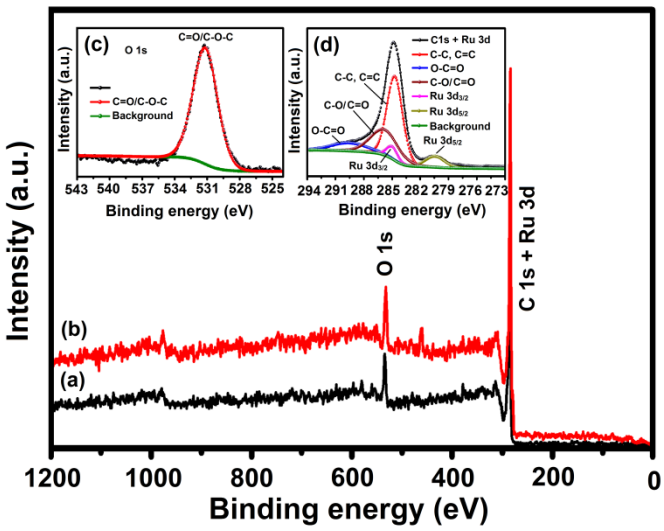

Fig. 4 XPS spectra of (a) CPM and (b) Ru/CPM-1, (c) Expanded XPS profiles in the (c) O 1s and (d) C1s+ Ru 3d regions of the Ru/CPM-1 nanocomposite.

Both samples show obvious peaks centered at the binding energies of around 532.3 eV, which was assigned to O 1s signal. The C1s signals at 284.8, 286.2, 287.4, and 289.1 eV corresponds to aromatic carbon groups (C-C/C=C), either hydroxyl or carbonyl groups (C-O/C=O), and carboxylic groups (O-C=O) are clearly observed, respectively. Obviously, we can see that the peak C1s (284.8 eV) corresponds to the graphitic carbon atoms in CPM was observed.[28] The signals of 284.8 and 280.0 eV are usually observed for the Ru $3d_{3/2}$ and Ru $3d_{5/2}$ photoelectron spectral lines for metallic ruthenium.[29]

3.2 Catalytic properties of Ru/CPM catalysts

3.2.1. Reduction of *p*-NA over Ru/CPM catalysts

To determine the catalytic properties of Ru/CPM catalysts, the reduction reaction of *p*-NA in the presence of Ru catalyst and $NaBH_4$ were carried out by monitored the reduction reaction using a UV-vis absorption spectrophotometer. Fig. 5 shows the temporal evolution of the absorption spectral changes of *p*-NA in the absence and presence of Ru/CPM catalysts. The absorption spectrum of *p*-NA with $NaBH_4$ mixture solution exhibits the longer wavelength band at 380 nm (Fig. 5a). It was observed that the solution color of *p*-NA and their absorbance at 380 nm remain unchanged with time, indicates that the reduction reaction rate was extremely slow.[30,31] Interestingly the addition of Ru/CPM catalysts into the mixture solution of *p*-NA with $NaBH_4$, the absorbance of *p*-NA at 380 nm was found to decreases with increasing time and concurrently

appearing a new absorption band at 310 nm and their absorbance increases with time as shown in Figs. 5b and 5c.

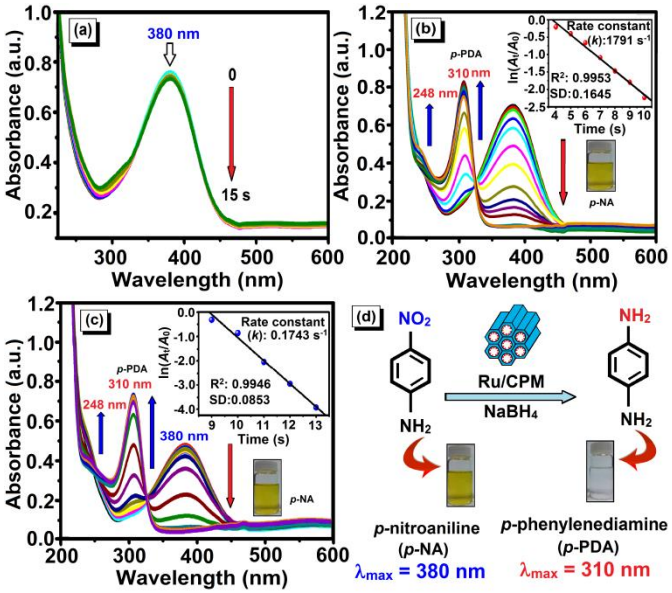

Fig. 5 (a) Absorption spectra of *p*-NA and $NaBH_4$ mixture solution after 15 s (without catalyst), (b) presence of Ru/CPM-1, (c) Ru/CPM-2 catalysts and (d) structural illustration of *p*-NA molecules in reduction reactions.

During the reduction reaction, the yellowish colored solution of *p*-NA was disappeared with time. The observed color change and decrease in absorbance at 380 nm is due to the formation *p*-PDA as a result of the reduction reaction between *p*-NA and Ru/CPM catalyst.[16] A new absorption band appeared at 310 nm is ascribed to the *p*-PDA product. The rate constant (*k*) for the reduction reaction of *p*-NA by Ru/CPM catalysts was obtained from the slope of the plot between $\ln(A_t/A_0)$ *versus* reaction time according to pseudo-first order kinetics rate constant equation with respect to *p*-NA can be written as

$$dC/dt = -kC \quad (2)$$

where *C* is the concentration of *p*-NA at time t and *k* is the rate constant. The above equation can also be expressed in terms of absorbance (*A*) i.e.

$$\ln(C_t/C_0) = \ln(A_t/A_0) = -kt \quad (3)$$

where A_t is the absorbance at time t and A_0 is the absorbance at time zero. The resulting plot shows linear behaviour for both Ru/CPM catalyst systems (inset Figs. 5b and 5c). The reaction rate constant was estimated to be 0.1791 s^{-1} (Ru/CPM-1) and 0.1743 s^{-1} (Ru/CPM-2), reveals that the Ru/CPM catalysts exhibit excellent catalytic performance for reduction reaction.

3.2.2 Proposed mechanism of *p*-NA over Ru/CPM catalyst

On the basis of the above results, and also in accordance with previous literature reports,[30b] a plausible reaction pathway for the reduction reaction of *p*-NA is proposed as shown in Scheme 2. In Step I, the formation of RuNPs is embedded on the surface of CPM frame work. Adsorption of *p*-NA onto the catalyst surface followed by interfacial electron transfer and desorption of *p*-NA away from the surface. Here, electron transfer from BH_4^- (Step II) to *p*-NA through adsorption of the reactant molecules onto the surface of the Ru/CPM catalyst (i.e. hydrogen atoms bound on the active surface of RuNPs, Step III). The adsorption process of substrates is driven by chemical interaction (chemisorption) between the particle surface and substrates. Finally, *p*-PDA was formed, followed by desorption of product from the metal surfaces (Step IV) and reactivation of the Ru/CPM catalytic system.[16] One of the main advantages of using heterogeneous catalyst systems that are greener, safer, environmentally friendly and reusable is a research priority particularly for the chemical, pharmaceutical and an industrial perspective applications.[16]

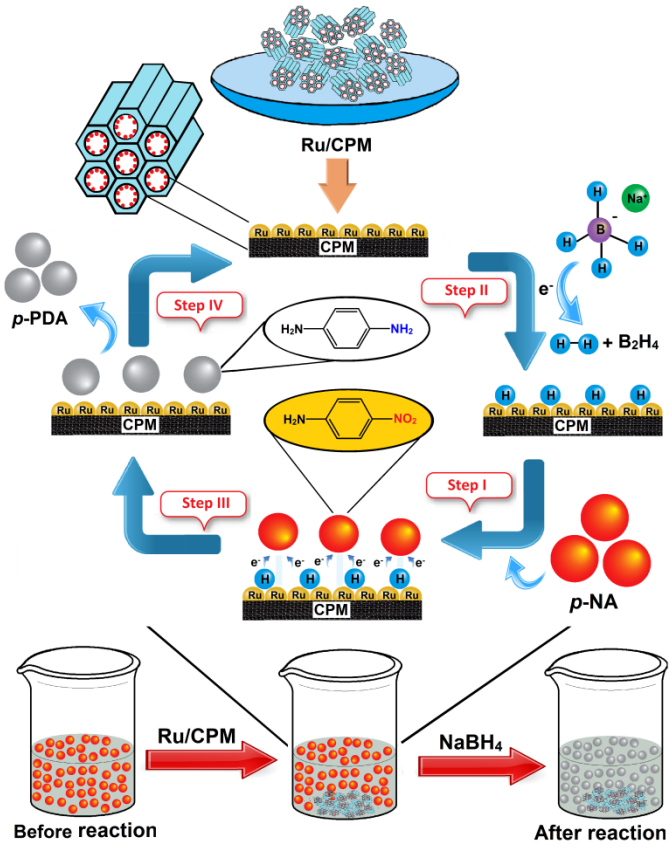

Scheme 2. The proposed mechanism of the reduction of *p*-NA by $NaBH_4$ using Ru/CPM catalyst. After reaction, Ru/CPM was easily recovered by centrifugation and reused.

3.2.3 Comparison for the reduction of *p*-NA with different catalysts

Over the past few decades, carbon-based nanocomposite materials have been explored as promising materials in the development for the reduction of 4-NA to *p*-PDA, using $NaBH_4$ as reductant.[32,33] As reflected in Table 2, preparation of graphene oxide (GO) and reduced graphene oxide (RGO) from graphite is an intricate procedure that may also lead to hazardous explosions.[32,33] On the other hand, the procedure for fabrication of CPMs from soft-templating method is simple and more environmentally friendly.

Table 2 Comparison of apparent rate constants of some recent carbon-based nanocatalysts with present work for reduction of *p*-NA by $NaBH_4$

Entry	Catalyst	Size (nm)	Catalyst amount (mg)	Time (s)	BET surface area ($m^2\ g^{-1}$)	Rate constant, *k* (s^{-1})	Reference
1	Pt/RG[a]	2–6	37.5 [μg mL^{-1}]	240	–	0.63[h]	32*a*
2	Au/GO[b]	5	600 [μL]	480	–	0.94[h]	32*b*
3	Ag/G[c]	100	100	960	40.3	0.0033	32*c*
4	Au/PRGO	1-30	3	360	204	–	32*d*
5	Au/RGO	50	12	270	–	0.008[h]	32*e*
6	Pt/GA[d]	~ 20	2	600	154	0.44[h]	33*a*
7	$Ag_{50}Ni_{50}$/RGO[e]	~ 11 ± 3	0.5	40	–	0.0565	33*b*
8	$Cu_{6/7}Co_{1/7}Fe_2O_4$/G[c]	20[f]	20	540	–	–	33*c*
9	Ru/CPM-1	2.6 ± 0.5	1	15	1416	0.1791	This work
10	Ru/CPM-2	2.8 ± 0.5	1	15	1313	0.1743	This work
11	Ru/CPM-1	2.6 ± 0.5	2	11	1416	0.1844	This work
12	Ru/CPM-1	2.6 ± 0.5	3	8	1416	0.1893	This work
13	Ru/CPM-1[g]	2.6 ± 0.5	3	8	1416	0.1862	This work

[a] RG: Reduced graphene. [b] GO: Graphene oxide. [c] G: Graphene. [d] GA: Graphene aerogel. [e] RGO: Reduced graphene oxide. [f] Reaction at 70 °C. [g] Excess of $NaBH_4$ used. [h] Unit: min^{-1}.

In addition, carbon porous materials, which have been used in several industrial applications, are known to have unique properties such as ultrahigh surface area, tailorable pore size, low toxicity, good electrical conductivity and high chemical stability.[1–7] Moreover, reaction was performed at room temperature for all the catalysts, except the $Cu_{6/7}Co_{1/7}Fe_2O_4$–graphene nanocatalyst,[33c] which was held at 70 °C, this is an another disadvantage compared to our catalyst systems.

3.2.4 Reduction of CV over Ru/CPM catalysts

A similar reduction pattern for CV dye was also observed in which the peak at 581 nm decreases with the increase in absorption at 260 nm, clearly indicating the formation of leuco crystal violet (LCV)[34] in the presence of Ru/CPM catalysts (Figs. 6a and 6b). No reaction happened in the absence of catalyst and reaction is going fast in the excess of reductant (Fig. S1, ESI†). During reduction reaction, the solution colour was changed from dark violet to colourless, indicates that the CV was reduced by Ru/CPM catalyst results in the formation of LCV as a products.[34] The rate constant for the reduction reaction of CV was calculated to be 0.2041 s^{-1} (Ru/CPM-1) and 0.2436 s^{-1} (Ru/CPM-2), reveals that these catalysts show an effective catalytic performance. The removal of CV from waste water is a major environmental problem and threat to the society. Recently, different approaches have been utilized to removal or degradation of CV dye containing the wastewater treatment.

3.2.5 Comparison for the reduction of CV with different catalysts

A number of articles describing the use of supported nanocomposites as catalysts for catalytic degradation and/or reduction of CV dye have been published.[35–38] The photocatalytic degradation reaction of CV using UV/H_2O_2,[35a] Fenton reagent (H_2O_2+Fe^{2+}) systems,[35b] Ag/TiO_2,[35c] CdS/Zeolite-A,[35d] and Sm_2InTaO_7[35e] have been studied. Likewise, microwave irradiation of spinal $CuFe_2O_4$ catalyst,[36a] sonochemical method,[36b] ozonation over Fe/activated carbon catalyst,[36c] oxidation by iron oxide-coated granular activated carbon (Fe_3O_4/GAC)[37] has been developed for the CV removal methods. The BET surface area of spinal $CuFe_2O_4$ and Fe_3O_4/GAC catalysts are 195 and 745 $m^2\ g^{-1}$ respectively, which are lower than that of compared to our catalyst systems.[36a] But the drawback of these systems is that more time is required for the reaction. The novelty of this catalyst system is that a lesser time (20 s) is needed to complete the reaction and also compared to the reported catalysts (Table 3).

Murugan and Shanmugam[37c] also studied the reduction of CV using the PS-PVBC-*g*-PAC-MNPs (MNPs = Ag, Pd and Au) catalysts and their corresponding pseudo-first-order-rate constants (*k*) 1.6.74 × 10^5, 2.546 × 10^5 and 8.45 × 10^4 s^{-1} were calculated. Among these, AuNPs containing catalyst shows more active than silver and palladium catalysts. A lesser quantity of catalyst (1 mg) is used for the reaction, compared to other catalyst systems reported. Based on the above results, it may conclude that the Ru/CPM catalysts exhibited excellent catalytic performance in the reduction of dyes.

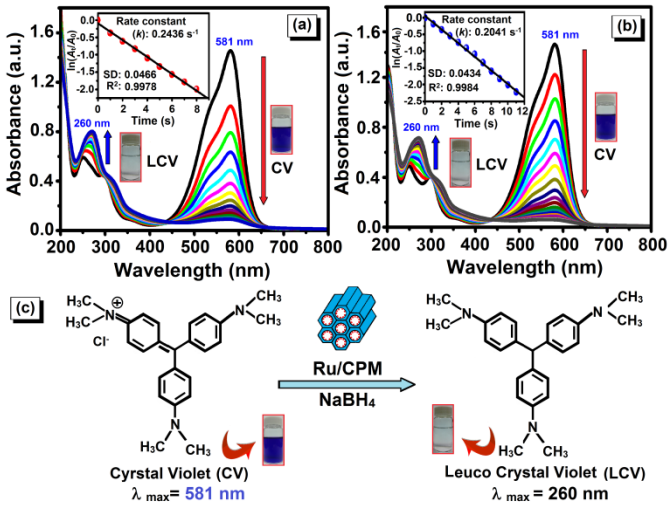

Fig. 6 (a) Absorption spectra of CV and $NaBH_4$ mixture solution in the presence of Ru/CPM-1, (b) Ru/CPM-2 catalysts and (c) structural illustration of CV dye.

A control experiment of adding $NaBH_4$ was performed in the same reaction conditions as in the absence of Ru/CPM-1 catalyst and excess of the reductant as shown in (Fig. S1 and S2, ESI†). We made an attempt to compare the catalytic activity of *p*-NA reduction were carried out with different amounts of the catalyst (Ru/CPM-1, 2.0 mg; Ru/CPM-1, 3.0 mg; Ru/CPM-1, 3.0 mg with excess $NaBH_4$) was added to the reaction mixture to check their kinetic reaction rates. Although increasing Ru/CPM-1 catalyst might increase the catalytic activity. This indicates that the increase in Ru/CPM-1 catalyst loading decrease the time period of reduction process and rate of reaction was calculated from $\ln(A_t/A_0)$ *vs* time (sec) in different time frames are shown in Fig. (Fig. S1 ESI†).[38a] It is well known that the reaction follows the pseudo-first order kinetics with respect to the concentration of *p*-NA when excess $NaBH_4$ was used.[38b] In this condition, the rate of the reaction was retarded, the fact is that the concentration of $NaBH_4$ increases the adsorption of *p*-NA and desorption of the products form the surface was too slow. The results indicate that reduction process follows a pseudo-first-order reaction with rate constant (k) = 0.1862 s^{-1}. This aspect can be studied in more details in the future. The reduction of CV in using $NaBH_4$ is quite slow if it is performed without using the catalyst. Initially, is slightly slower and after some time the reaction become faster in the excess of $NaBH_4$. Pal and co-workers report that the reaction rate increases with an increase in surface area of the catalyst.[39] Different amount of the Ru/CPM-1 catalyst (2.0 and 3.0 mg) added to the reaction mixture and the reduction of CV can be examined by UV-visible spectrophotometer and their pseudo-first-order rate constant of the reactions are shown in Fig. S3, ESI†.

On the other hand, the rate constant of Ru/C was calculated to be a lower (k = 0.0298 s^{-1}) compared with present catalyst (data not shown); they needed more than 6 times to achieve a similar rate constant to that obtained with the Ru/CPM-1 catalyst. Because of Ru/C has lower surface area and its catalytic activity compared to present system. It was noted and interesting that the Due to their promising properties of Ru/CPM, it can be utilized to fabricate 3D carbon-based materials for a variety of novel applications. In addition, the CV reaction using Ru/CPMs catalysts show the following advantages: (i) a simple work-up procedure and reusability of the catalyst, (ii) high surface area and porous structure, (iii) simple and low-cost method and attracts much attention, and (iv) lesser quantity required for the reaction. Another befitting application of this catalyst system is in environmental remediation utilizing Ru/Carbon-based technologies. Moreover, in this work, the Ru/CPM-1 catalyst was found to be a better for the catalytic reduction of *p*-NA and CV dye molecules.

Table 3 Summary of reports in the literature on CV based over various catalytic systems

Entry	Catalyst	Size (nm)	Method	Source/reagent	Time (s)	Rate constant, k (s^{-1})	Reference
1	CdS/Zeolite A	48–68	Photodecolorization	Sun-light	1500	–	35*d*
2	Sm_2InTaO_7	1000	Photodegradation	UV Lamp	3600	–	35*e*
3	$CuFe_2O_4$	50–100	Microwave radiation	–	5400	0.0057	36*a*
4	Fe/AC[a]	250–300	Ozonation	O_3[d]	1800	–	36*c*
5	Fe_3O_4/GAC[b]	> 100	Oxidation	H_2O_2	10800	–	36*a*
6	PS–PVBC-*g*-PAC[c]–AgNPs	20–25	Reduction	$NaBH_4$	1800	1.674×10^5	37*c*
7	PS–PVBC-*g*-PAC[c]–PdNPs	20–25	Reduction	$NaBH_4$	1800	8.45×10^4	37*c*
8	PS–PVBC-*g*-PAC[c]–AuNPs	20–25	Reduction	$NaBH_4$	1800	2.546×10^5	37*c*
9	Ru/CPM-1	2.6 ± 0.5	Reduction	$NaBH_4$	30 s	0.2041	This work
10	Ru/CPM-2	2.6 ± 0.5	Reduction	$NaBH_4$	30s	0.2436	This work
11	Ru/CPM-1	2.6 ± 0.5	Reduction	$NaBH_4$	25s	0.2461	This work
12	Ru/CPM-1	2.6 ± 0.5	Reduction	$NaBH_4$	20s	0.2487	This work

[a] AC: Activated carbon. [b] GAC: Granular activate carbon. [c] PS–PVBC-*g*-PAC: Poly(styrene)-co-(vinyl benzyl chloride) grated 2-acryloxyethyltrimethyl ammonium chloride (PAC). [d] O_3: Ozone.

3.2.6 Stability of the Ru/CPM catalysts

For practical applications, the reusability of the catalyst is an important factor for heterogeneous systems. To study the catalyst stability, the catalyst was centrifuged after reaction, and the clear supernatant liquid was decanted carefully. The catalyst was washed thoroughly with DI water and ethanol, followed by drying at 60 ^{o}C for 6 h in vacuum oven. Then, the catalyst was reused for subsequent recycle under the same reaction conditions. It can be observed that the rate constant (*k*) values are decreased after the consecutive cycle as shown in Fig. 7a. The slight changes in (*k*) values are probably due to the loss of some catalyst at the time of centrifugation or transferring the catalyst during the reaction time. After the fifth run, to check their stability of the recovered Ru/CPM-1 catalyst was examined by XRD and FE-TEM analysis (Fig. 7.) Compared with XRD and FE-TEM images of the fresh (Figs. 2c-f) and recycled catalyst (Figs. 7c,d) do not show any obvious changes and could be reused without significant loss of catalytic activity, which indicated that the Ru/CPM-1 catalyst had a good stability. Notably, it is observed that the shape and size (*ca.* 2–3 nm) of the Ru NPs remain unchanged with spherical morphologies and support the proposal that the morphology of the catalyst remains the same even in the used conditions. Moreover, these results indicate that the present catalysts (Ru/CPMs) systems are good for reduction reactions. It proves that the Ru/CPM catalysts are highly effective and stable catalysts with great potential applications.

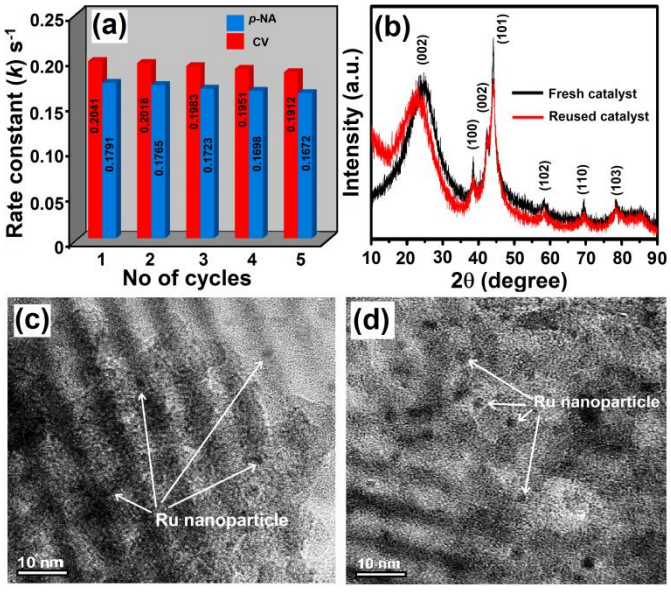

Fig. 7 (a) The kinetic rate constant (*k*) of *p*-NA and CV for each cycle, (b) XRD spectra and (c,d) High-resolution FE-TEM images of Ru/CPM-1 catalyst after fifth cycle.

From these analyses further indicated that the RuNPs incorporation inside the 3D carbon support could efficiently stabilize RuNPs and also prevent their aggregation and good stability.

4. Conclusions

In summary, we have demonstrated and characterized a stable 3D mesoporous carbon which functions as a good support for RuNPs (Ru/CPMs). These catalysts have high surface area and were used as a heterogeneous catalyst for the reduction reactions. The Ru/CPM-1 catalyst exhibited much higher catalytic activity than that of the Ru/CPM-2 catalyst. The pseudo-first-order rate constant (*k*) estimated for the reduction of *p*-NA and CV dye molecules were discussed. It was shown that the catalytic activity of Ru/CPM system was discussed in terms of amount of catalyst and the number of consecutive catalytic cycles. Moreover, the stability of the catalyst was examined by with XRD and FE-TEM images of the system before and after catalytic process. Due to ultra-high surface area, pore volume and well-defined pore size of the 3D CPM matrix, which may enhances the absorption abilities; reactants can easily gain access to the surface of the RuNPs and helps to promoting the reduction reaction. These unique features of these catalytic systems might be potentially important for applications in chemical industries. Further the application of this catalytic system towards many other key transformations is currently being explored.

Acknowledgements

The financial supports for this work by the Ministry of Science and Technology (MOST), Taiwan (NSC101-2113-M-001-020-MY3 to SBL) is gratefully acknowledged.

References

1 (*a*) Z. Ji, S. Liang, Y. Jiang, H. Li, Z. Liu and T. Zhao, *Carbon*, 2009, **47**, 2194–2199; (*b*) G. Lan, H. Tang, Y. Zhou, W. Han, H. Liu, X. Li and Y. Li, *ChemCatChem*, 2014, **6**, 353–360; (*c*) Q. Wang, W. Zhang, Y. Mu, L. Zhong, Y. Meng and Y. Sun, *Micropor. Mesopor. Mater.*, 2014, **197**, 109–115; (*d*) L. Shang, T. Bian, B. Zhang, D. Zhang, L. Z. Wu, C. H. Tung, Y. Yin and T. Zhang, *Angew. Chem. Int. Ed.*, 2014, **53**, 250–254.

2 (*a*) T. Y. Ma, L. Liu and Z. Y. Yuan, *Chem. Soc. Rev.*, 2013, **42**, 3977–4003; (*b*) T. Parsons-Moss, J. Wang, S. Jones, E. May, D. Olive, Z. Dai, M. Zavarin, A. B. Kersting, D. Zhao and H. Nitsche, *J. Mater. Chem. A*, 2014, **2**, 11209–11221; (*c*) Y. Zhai, Y. Dou, D. Zhao, P. F. Fulvio, R. T. Mayes and S. Dai, *Adv. Mater.*, 2011, **23**, 4828–4850; (*d*) C. Liang, Z. Li and S. Dai, *Angew. Chem. Int. Ed.*, 2008, **47**, 3696–3717.

3 (*a*) D. S. Su, S. Perathoner and G. Centi, *Chem. Rev.*, 2013, **113**, 5782−5816; (*b*) L. B. Sun, X. Q. Liu and H. C. Zhou, *Chem. Soc. Rev.*, 2015, **44**, 5092−5147; (*c*) P. Veerakumar, R. Madhu, S. M. Chen, C. T. Hung, P. H. Tang, C. B. Wang and S. B. Liu, *Analyst*, 2014, **139**, 4994–5000; (*d*) P. Veerakumar, R. Madhu, S. M. Chen, C. T. Hung, P. H. Tang, C. B. Wang and S. B. Liu, *J. Mater. Chem. A*, 2014, **2**, 16015–16022; (*e*) Y. Ding, X. Li, H. Pan and P. Wu, *Catal. Lett.*, 2014, **144**, 268–277; (*f*) J. Zhu, A. Holmen and D. Chen, *ChemCatChem*, 2013, **5**, 378–401.

4 (*a*) Y. Deng, Y. Cai , Z. Sun, D. Gu, J. Wei, W. Li, X. Guo, J. Yang and D. Zhao, *Adv. Funct. Mater.*, 2010, **20**, 3658–3665; (*b*) Y. Chen and Y. Liu, *J. Mater. Chem. A*, 2014, **2**, 9193–9199.

5 (*a*) R. T. Mayes, C. Tsouris, J. O. Kiggans Jr., S. M. Mahurin, D. W. DePaoli and S. Dai, *J. Mater. Chem.*, 2010, **20**, 8674–8678; (*b*) P. F. Fulvio, S. S. Brown, J. Adcock, R. T. Mayes, B. Guo, X. G. Sun, S. M. Mahurin, G. M. Veith and S. Dai, *Chem. Mater.*, 2011, **23**, 4420–4427.

6 (*a*) X. Wang, J. S. Lee, C. Tsouris, D. W. DePaoli and S. Dai, *J. Mater. Chem.*, 2010, **20**, 4602–4608. (*b*) Y. Meng, D. Gu, F. Zhang, Y. Shi, H.

Yang, Z. Li, C. Yu, B. Tu and D. Zhao, *Angew. Chem., Int. Ed.*, 2005, **44**, 7053–7059; (*c*) A. P. Katsoulidis and M. G. Kanatzidis, *Chem. Mater.*, 2011, **23**, 1818–1824; (*d*) Z. Sun, B. Sun, M. Qiao, J. Wei, Q. Yue, C. Wang, Y. Deng, S. Kaliaguine and D. Zhao, *J. Am. Chem. Soc.*, 2012, **134**, 17653–17660.

7 (*a*) K. Kusada, H. Kobayashi, T. Yamamoto, S. Matsumura, N. Sumi, K. Sato, K. Nagaoka, Y. Kubota and H. Kitagawa, *J. Am. Chem. Soc.*, 2013, **135**, 5493−5496; (*b*) G. Chen, J. Zhang, A. Gupta, F. Rosei and D. Ma, *New J. Chem.*, 2014, **38**, 1827−1833; (*c*) J. Ohyama, T. Sato, Y. Yamamoto, S. Arai and A. Satsuma, *J. Am. Chem. Soc.*, 2013, **135**, 8016−8021; (*d*) Y. Yang, C. J. Sun, Y. Ren, S. J. Hao and D. Q. Jiang, *Sci. Rep.*, 2014, **4**, 4540; (*e*) P. Tomkins, E. Gebauer-Henke, W. Leitner and T. E. Müller, *ACS Catal.*, 2015, **5**, 203−209.

8 X. Y. Quek, R. Pestman, R. A. van Santen and E. J. M. Hensen, *Catal. Sci. Technol.*, 2014, **4**, 3510–3523.

9 N. Saadatjou, A. Jafari and S. Sahebdelfar, *Chem. Eng. Commun.*, 2015, **202**, 420−448.

10 P. Das, N. Aggarwal and N. R. Guha, *Tetrahedron Lett.*, 2013, **54**, 2924−2928.

11 P. Veerakumar, S. Balakumar, M. Velayudham, K. L. Lu and S. Rajagopal, *Catal. Sci. Technol.*, 2012, **2**, 1140–1145.

12 (*a*) J. L. Castelbou, E. Bres-Femenia, P. Blondeau, B. Chaudret, S. Castilln, C. Claver and C. Godard, *ChemCatChem*, 2014, **6**, 3160–3168; (*b)* S. Xu, P. Zhang, H. Li, H. Wei, L. Li, B. Li and X. Wang, *RSC Adv.*, 2014, **4**, 7079–7083; (*c*) N. C. Antonels and R. Meijboom*, Langmuir*, 2013, **29**, 13433–13442.

13 A. I. Carrillo, L. C. Schmidt, M. L. Marín and J. C. Scaiano, *Catal. Sci. Technol.*, 2014, **4**, 435–440.

14 (*a*) N. Tonanon, Y. Wareenin, A. Siyasukh, W. Tanthapanichakoon, H. Nishihara, S. R. Mukai and H. Tamon, *J. Non-Crystalline Solids*, 2006, **352**, 5683–5686; (*b*) L. Zubizarreta, A. Arenillas, J. A. Menéndez, J. J. Pis, J. P. Pirard and N. Job, *J. Non-Crystalline Solids*, 2008, **354**, 4024–4026; (*c*) E. G. Calvo, E. J. Juárez-Pérez, J. A. Menéndez and A. Arenillas, *J. Colloid Inter. Sci.*, 2011, **357**, 541–547. (*d*) L. Zubizarreta, A. Arenillas, A. Domínguez, J. A. Menéndez and J. J. Pis, *J. Non-Crystalline Solids*, 2008, **354**, 817–825; (*e*) J. A. Menéndez, E. J. Juárez-Pérez, E. Ruisánchez, E. G. Calvo and A. Arenillas, *Carbon*, 2012, **50**, 3555–3560.

15 (*a*) J. H. Zhou, J. P. He, Y. J. Ji, W. J. Dang, X. L. Liu, G. W. Zhao, C. X. Zhang, J. S. Zhao, Q. B. Fu and H. P. Hu, *Electrochimica Acta*, 2007, **52**, 4691–4695; (*b*) L. C. Sang, A. Vinu and M. O. Coppens, *J. Mater. Chem.*, 2011, **21**, 7410–7417; (*c*) L. Chen, X. Cui, M. Wang, Y. Du, X. Zhang, G. Wan, L. Zhang, F. Cui, C. Wei and J. Shi, *Langmuir*, 2015, **31**, 7644−7651.

16 (*a*) S. Kundu, K. Wang and H. Liang, *J. Phys. Chem. C*, 2009, **113**, 5157–5163; (*b*) F. Guo, Y. Ni, Y. Ma, N. Xiang and C. Liu, *New J. Chem.*, 2014, **38**, 5324−5330; (*c*) T. Aditya, A. Pal and T. Pal, *Chem. Commun.,* 2015, **51**, 9410−9431.

17 (*a*) R. A. Smiley, in *Phenylene and Toluenediamines*, John Wiley & Sons, Inc., New York, 2000; (*b*) I. Yoshiaki and K. J. Masa-aki, *Health Sci.*, 2000, **46**, 467−473; (*c*) H. S. Lee and Y. W. Lin, *Ann. Occup. Hyg.*, 2009, **53**, 289−296.

18 (*a*) K. Mohanty, J. T. Naidu, B. C. Meikap and M. N. Biswas, *Ind. Eng. Chem. Res.*, 2006, **45**, 5165−5171; (*b*) Z. Chen, T. Wang, X. Jin, Z. Chen, M. Megharaj and R. Naidu, *J. Colloid Interface Sci.*, 2013, **398**, 59–66; (*c*) H. He, S. Yang, K. Yu, Y. Ju, C. Sun and L. Wang, *J. Hazard. Mater.*, 2010, **173**, 393–400; (*d*) H. J. Fan, C. S. Lu, W. L. W. Lee, M. R. Chiou and C. C. Chen, *J. Hazard. Mater.*, 2011, **185**, 227–235.

19 (*a*) J. W. Churchman, *J. Experi. Med.*, 1912, **16,** 221–247; (*b*) N. A. Littlefield, B. N. Blackwell, C. C. Hewitt and D. W. Gaylor, *Fundam. Appl. Toxicol.*, 1985, **5**, 902–912.

20 S. Gupta, C. Giordano, M. Gradzielski and S. K. Mehta, *J. Colloid Inter. Sci.*, 2013, **411**, 173–181.

21 F. A. Pavan, E. S. Camacho, E. C. Lima, G. L. Dotto, V. T. A. Branco and S. L. P. Dias, *J. Enviro. Chem. Eng.*, 2014, **2**, 230–238.

22 P. K. Tripathi, M. Liu, Y. Zhao, X. Ma, L. Gan, O. Noonan and C. Yu, *J. Mater. Chem. A*, 2014, **2**, 8534–8544.

23 (*a*) W. J. Bodziak, *Forensic Sci. Int.*, 1996, **82**, 45–52; (*b*) L. Spence and G. Asmussen, *Forensic Sci. Int.*, 2003, **132**, 117–124; (*c*) A. L. Michaud and L. Brun-Conti, *J. Forensic Sci. Int.*, 2004, **49**, 511–516; (*d*) K. J. Farrugia, K. A. Savage, H. Bandey, T. Ciuksza and N. N. Daéid, *Sci. Justice*, 2011, **51**, 110–121.

24 (*a*) A. C. Ferrari and J. Robertson, *Phys. Rev. B: Condens. Matter.*, 2000, **61,** 14095–14107; (*b*) X. R. Wen, D. S. Zhang, T. T. Yan, J. P. Zhang and L. Y. Shi, *J. Mater. Chem. A*, 2013, **1**, 12334–12344; (*c*) M. S. Nashner, A. I. Frenkel, D. L. Adler, J. R. Shapley and R. G. Nuzzo, *J. Am. Chem. Soc.*, 1997, **119**, 7760–7771.

25 F. Liu, C. Li, L. Ren, X. Meng, H. Zhang and F. S. Xiao, *J. Mater. Chem.*, 2009, **19**, 7921–7928.

26 C. M. Ghimbeu, L. Vidal, L. Delmotte, J. M. L. Meins and C. Vix-Guterl, *Green Chem.*, 2014, **16**, 3079–3088.

27 (*a*) Y. Meng, D. Gu, F. Zhang, Y. Shi, L. Cheng, D. Feng, Z. Wu, Z. Chen, Y. Wan, A. Stein and D. Zhao, *Chem. Mater.*, 2006, **18**, 4447−4464; (*b*) I. Ogino, S. Kazuki and S. R. Mukai, *J. Phys. Chem. C*, 2014, **118**, 6866−6872.

28 G. Li, H. Nagasawa, M. Kanezashi, T. Yoshioka and T. Tsuru, *J. Mater. Chem. A*, 2014, **2**, 9185–9192.

29 *Handbook of X-ray Photoelectron Spectroscopy*, Eds. C. D. Wagner, W. M. Riggs, L. E. Davis, J. E. Moulder and G. E. Muilenberg, Perkin-Elmer Corp., Eden Prairie, MN, 1979.

30 (*a*) M. Chirea, A. Freitas, B. S. Vasile, C. Ghitulica, C. M. Pereira and F. Silva, *Langmuir*, 2011, **27**, 3906–3913; (*b*) U. Nithiyanantham, S. R. Ede and S. Kundu, *J. Mater. Chem. C*, 2014, **2**, 3782–3794.

31 N. Pradhan, A. Pal and T. Pal, *Colloids and Surfaces A*, 2002, **196**, 247−257.

32 (*a*) M. M. Raju and D. K. Pattanayak, *RSC Adv.*, 2015, **5**, 59541–59549; (*b*) K. Jasuja, J. Linn, S. Melton and V. Berry, *J. Phys. Chem. Lett.*, 2010, **1**, 1853–1860; (*c*) Y. Chu, Z. Wang, and Q. Pan, *ACS Appl. Mater. Interfaces*, 2014, **6**, 8378−8386; (*d*) M. Q. Yang, X. Pan, N. Zhang and Y. J. Xu, *CrystEngComm*, 2013, **15**, 6819–6828; (*e*) B. Adhikari, A. Biswas and A. Banerjee, *ACS Appl. Mater. Interfaces*, 2012, **4**, 5472−5482.

33 (*a*) X. Zhang, D. Liu, L. Yang, L. Zhou and T. You, *J. Mater. Chem. A*, 2015, **3**, 10031–10037; (*b*) R. Dhanda and M. Kidwai, *J. Mater. Chem. A*, 2015, **3**, 19563−19567; (*c*) H. Zhang, Y. Zhao, W. Liu, S. Gao, N. Shang, C. Wang and Z. Wang, *Catal. Commun.*, 2015, **59**, 161–165.

34 M. Mittal, M. Sharma and O. P. Pandey, *J. Nanosci. Nanotech.*, 2014, **14**, 2725–2733.

35 (*a*) F. A. Alshamsi, A. S. Albadwawi, M. M. Alnuaimi, M. A. Rauf and S. S. Ashraf, *Dyes Pigments*, 2007, **74**, 283−287; (*b*) H. J. Fan, S. T. Huang, W. H. Chung, J. L. Jan, W. Y. Lin and C. C. Chen, *J. Hazard. Mater.*, 2009, **171**, 1032–1044; (*c*) S. Samira, P. Akash Raja, C. Mohan and J. M Modak, *J. Thermodynam. Cat.,* 2012, **3**, 117; (*d*) A. Nezamzadeh-Ejhieh and Z. Banan, *Desalination*, 2011, **279**, 146–151; (*e*) L. M. Torres-Marítnez, E. Moctezuma, M. A. Ruiz-Gómez, I. Juárez-Ramírez, M. Z. Figueroa-Torres, *Res. Chem. Intermed.*, 2013, **39**, 1533–1544.

36 (*a*) H. Chen, S. Yang, J. Chang, K. Yu, D. Li, C. Sun and A. Li, *Chemosphere*, 2012, **89**, 185–189; (*b*) F. Guzman-Duque, C. Pétrier, C. Pulgarin, G. Peñuela and R. A. Torres-Palma, *Ultrason Sonochem.*, 2011, **18**, 440–446; (*c*) J. Wu, H. Gao, S. Yao, L. Chen, Y. Gao and H. Zhang, *Sep. Puri. Tech.*, 2015, **147**, 179–185.

37 (*a*) C. C. Chen, W. C. Chen, M. R. Chiou, S. W. Chen, Y. Y. Chen and H. J. Fan, *J. Hazard. Mater.*, 2011, **196**, 420–425; (*b*) G. Ovejero, A. Rodríguez, A. Vallet and J. García, *Appl. Catal. B*, 2012, **125**, 166–171; (*c*) E. Murugan and P. Shanmugam, *Bull. Mater. Sci.*, 2015, **38**, 629–637.

38 (*a*) S. Kundu, S. Lau and H. Liang, *J. Phys. Chem. C*, 2009, **113**, 5150–5156; (*b*) J. F. Huang, S. Vongehr, S. C. Tang, H. M. Lu and X. K. Meng, *J. Phys. Chem. C*, 2010, **114**, 15005–15010.

39 (*a*) S. Jana, S. Pande, S. Panigrahi, S. Praharaj, S. Basu, A. Pal and T. Pal, *Langmuir*, 2006, **22**, 7091–7095; (*b*) S. Panigrahi, S. Basu, S. Praharaj, S. Pande, S. Jana, A. Pal, S. K. Ghosh and T. Pal, *J. Phys. Chem. C*, 2007, **111**, 4596–4605; (*c*) S. Saha, A. Pal, S. Kundu, S. Basu and T. Pal, *Langmuir*, 2010, **26**, 2885–2893.

Graphical Abstract

Title: Highly stable ruthenium nanoparticles on 3D mesoporous carbon: An excellent opportunity for the reduction reactions†

Author: Pitchaimani Veerakumar,[a] Namasivayam Dhenadhayalan,[b] King-Chuen Lin[b] and Shang-Bin Liu [*a,c]

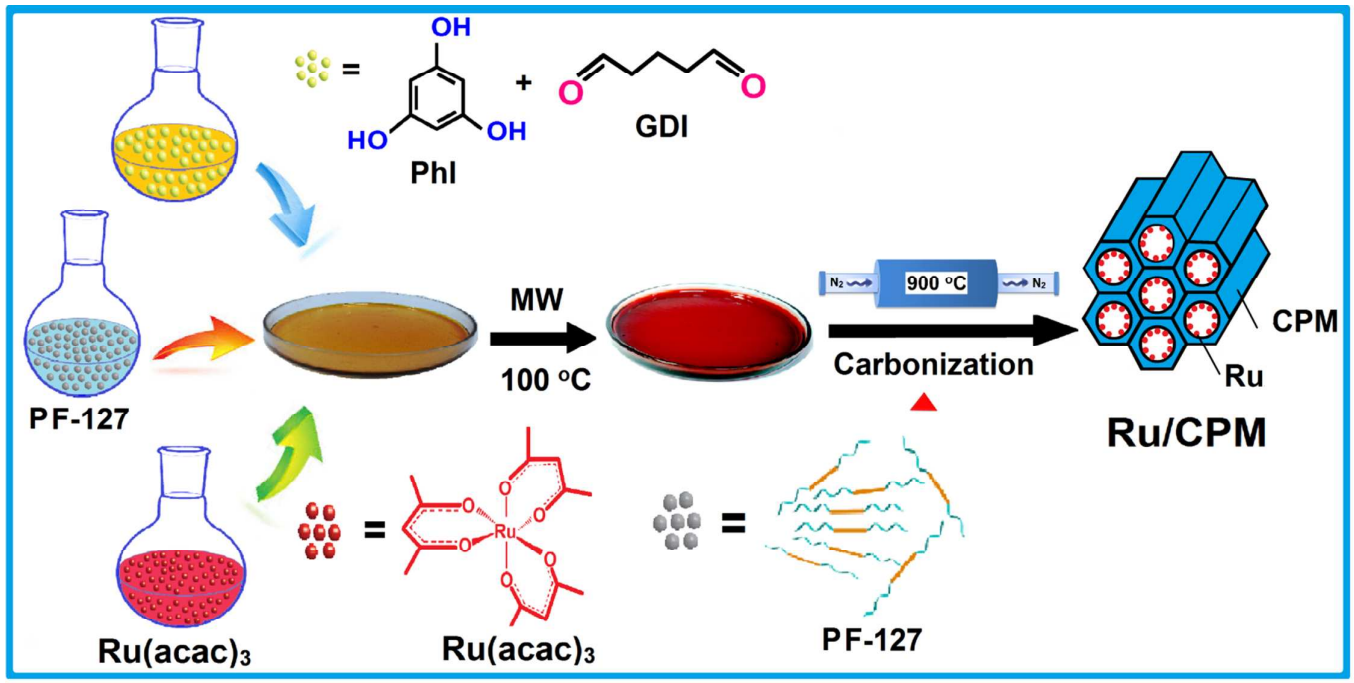

Highly dispersed Ru nanoparticles containing 3D mesoporouscarbon materials show superior performances during catalytic reduction of *p*-nitroaniline (*p*-NA) and crystal violet (CV) are studied.